Asia-Pac. J. Atmos. Sci., 54(1), 1-17, 2018
DOI:10.1007/s13143-017-0049-9

pISSN 1976-7633 / eISSN 1976-7951

Effect of Data Assimilation Parameters on The Optimized Surface CO_2 Flux in Asia

Hyunjung Kim[1], Hyun Mee Kim[1], Jinwoong Kim[1], and Chun-Ho Cho[2]

[1]*Atmospheric Predictability and Data Assimilation Laboratory, Department of Atmospheric Sciences, Yonsei University, Seoul, Korea*
[2]*National Institute of Meteorological Sciences, Seogwipo, Jeju, Korea*

(Manuscript received 28 October 2016; accepted 11 April 2017)

Abstract: In this study, CarbonTracker, an inverse modeling system based on the ensemble Kalman filter, was used to evaluate the effects of data assimilation parameters (assimilation window length and ensemble size) on the estimation of surface CO_2 fluxes in Asia. Several experiments with different parameters were conducted, and the results were verified using CO_2 concentration observations. The assimilation window lengths tested were 3, 5, 7, and 10 weeks, and the ensemble sizes were 100, 150, and 300. Therefore, a total of 12 experiments using combinations of these parameters were conducted. The experimental period was from January 2006 to December 2009. Differences between the optimized surface CO_2 fluxes of the experiments were largest in the Eurasian Boreal (EB) area, followed by Eurasian Temperate (ET) and Tropical Asia (TA), and were larger in boreal summer than in boreal winter. The effect of ensemble size on the optimized biosphere flux is larger than the effect of the assimilation window length in Asia, but the importance of them varies in specific regions in Asia. The optimized biosphere flux was more sensitive to the assimilation window length in EB, whereas it was sensitive to the ensemble size as well as the assimilation window length in ET. The larger the ensemble size and the shorter the assimilation window length, the larger the uncertainty (i.e., spread of ensemble) of optimized surface CO_2 fluxes. The 10-week assimilation window and 300 ensemble size were the optimal configuration for CarbonTracker in the Asian region based on several verifications using CO_2 concentration measurements.

Key words: Surface CO_2 flux, data assimilation parameters, CarbonTracker, ensemble Kalman filter

1. Introduction

Recently, the global monthly averaged atmospheric CO_2 concentration surpassed 400 ppm for the first time (Betts et al., 2016; WMO, 2016), which is a much larger magnitude compared with the CO_2 concentration in the early industrial revolution (approximately 280 ppm). Based on the fifth report of the Intergovernmental Panel on Climate Change (IPCC), CO_2 exerts the largest positive radiative forcing among all the major factors of climate change. Thus, it is necessary to understand the spatial-temporal distribution of atmospheric CO_2 concentrations. The distribution of atmospheric CO_2 concentrations can be quantitatively estimated by evaluating the surface CO_2 fluxes. The "bottom-up" approach can be used to estimate surface CO_2 flux, which is based on the directly measured flux observations or an ecosystem modeling (e.g., Krinner et al., 2005). In addition, the surface CO_2 flux can be estimated inversely using observed atmospheric CO_2 concentrations as a constraint (Enting, 2002). This inverse method is called the "top-down" approach and enables the effective estimation of surface (i.e., land and ocean) flux values based on limited observations (e.g., Gurney et al., 2002; Chevallier et al., 2010).

To improve the accuracy of surface CO_2 flux estimates and reduce their uncertainties, data assimilation methods used in Numerical Weather Prediction (NWP) have been applied. Several studies have estimated surface CO_2 fluxes using the variational method (e.g., Chevallier et al., 2005; Baker et al., 2006; Engelen et al., 2009; Basu et al., 2013) and the ensemble Kalman filter (EnKF) (e.g., Peters et al., 2005, 2007, 2010; Feng et al., 2009; Chatterjee et al., 2012). In the EnKF, the parameters (e.g., assimilation window length and ensemble size) used for data assimilation affect the results (Park and Kim, 2010). In Chatterjee et al. (2013), the inversion results obtained by four-dimensional variational (4DVAR) data assimilation showed more reliable large-scale source-sink patterns than those obtained by the EnKF; however, 4DVAR and EnKF results were similar when the number of ensembles in the EnKF increased. Babenhauserheide et al. (2015) demonstrated similar qualities for 4DVAR and EnKF analyses in regions with high observation densities, but for regions with sparse observations (e.g., Asia), there are large differences, which implies that there are large uncertainties in estimating the surface CO_2 fluxes in Asia. In addition, Babenhauserheide et al. (2015) suggested that longer assimilation window lengths add valuable information to the data assimilation system. Therefore, it is important to set appropriate data assimilation parameters (i.e., assimilation window length and ensemble size) when applying the EnKF method for estimating surface CO_2 fluxes, especially for the Asian region, where observations are distributed relatively sparsely.

The Earth System Research Laboratory at the National Oceanic and Atmospheric Administration (NOAA-ESRL) developed CarbonTracker, an inverse modeling system based on the EnKF, to estimate surface CO_2 fluxes. CarbonTracker has

Corresponding Author: Hyun Mee Kim, Department of Atmospheric Sciences, Yonsei University, 50 Yonsei-ro, Seodaemun-gu, Seoul 03722, Korea.
E-mail: khm@yonsei.ac.kr

been successfully applied for North America, Europe (Peters et al., 2007, 2010), and Asia (Kim et al., 2012, 2014a, 2014b, 2017; Zhang et al., 2014a, 2014b; Kim et al., 2016). For previous studies, a 5-week assimilation window and 150 ensemble members were used for all regions. However, as noted by Peters et al. (2007), surface CO_2 flux patterns in Asia may not be fully analyzed with a short assimilation window length (i.e., 5 weeks) because observations are sparsely distributed in Asia compared to North America and Europe. Therefore, finding the optimal parameters for data assimilation in the Asian region is necessary. In this study, several experiments with different assimilation window lengths and ensemble sizes were conducted, and the results were analyzed to find the optimal assimilation window length and ensemble size for the Asian region.

Section 2 presents a brief description of the CarbonTracker and EnKF, observations, and the experimental framework. In Section 3, the results are analyzed and an optimal set of parameters for the Asian region is estimated by comparing the results with several CO_2 measurements. Finally, Section 4 presents the summary and conclusion.

2. Methodology

a. CarbonTracker

CarbonTracker is a system for estimating the surface CO_2 flux using flux modules, observed atmospheric CO_2 concentrations, an atmospheric transport model (i.e., TM5), and the EnKF data assimilation system (Peters et al., 2005, 2007). In CarbonTracker, the surface CO_2 flux is estimated by multiplying the optimized scaling factor (λ_r) to a prior flux instead of estimating the surface CO_2 flux directly. The prior surface CO_2 flux consists of biosphere flux (F_{bio}), ocean flux (F_{ocean}), fire flux (F_{fire}), and fossil fuel flux (F_{ff}), as in Eq. (1). The prior and optimized fluxes (F) are calculated at $1^o \times 1^o$ resolution.

$$F(x, y, t) = \lambda_r \cdot F_{bio}(x, y, t) + \lambda_r \cdot F_{ocean}(x, y, t) + F_{fire}(x, y, t) + F_{ff}(x, y, t) \quad (1)$$

where x and y denote the zonal and meridional grid points, respectively; t denotes time; λ_r represents the scaling factor corresponding to the r-th optimization region.

The biosphere flux and the fire flux were obtained from the Carnegie-Ames-Stanford Approach Global Fire Emissions Database (CASA-GFED), version 3.1 (van der Werf et al., 2010). Note that the fire flux represents only the direct CO_2 emissions caused by burning, whereas the subsequent effects of burning are included in the biosphere flux, which implies that slight variations in the fire flux can cause great uncertainty in the biosphere flux. In CarbonTracker, the fire flux is fixed to a prior flux value although the uncertainty of the fire flux cannot be neglected in Tropical Asia (e.g., van der Werf et al., 2010), whereas the biosphere flux is optimized by the assimilation process. The ocean flux was obtained from Jacobson et al. (2007), and the fossil fuel flux was obtained from the Carbon Dioxide Information and Analysis Center (CDIAC, Boden et al., 2010) and the Emission Database for Global Atmospheric Research (EDGAR, European Commission, 2009) inventories. The fossil fuel fluxes are spatially distributed in two steps: first, the coarse scale flux distribution country totals from CDIAC are mapped onto a $1^o \times 1^o$ grid; next, the totals within the countries are distributed according to the spatial patterns from the EDGAR inventories (Peters et al., 2007). In the case of fossil fuel, the prior flux is used intact because the estimations of inventory-based fossil fuel flux emissions are relatively reliable although the reliability is small in China (Liu et al., 2015). As a result, among the four flux modules, only the scaling factors for the biosphere and ocean fluxes are optimized through the EnKF data assimilation process.

The scaling factors optimized through data assimilation are the weekly basis linear parameters that correspond to the optimization regions which divide the globe in 156 regions. The optimization regions adopt different classifications for land and ocean. A total of 126 ecoregions are used for land with a combination of Transcom regions (Gurney et al., 2002) and ecosystem types from Olson et al. (1985), and the ocean is divided into 30 regions. The optimized flux is calculated by multiplying the scaling factor representing each optimization region to the prior surface flux.

Atmospheric CO_2 concentrations are calculated from the optimized surface CO_2 fluxes using a transport model, TM5 (Krol et al., 2005). TM5 is an off-line model with a 2-way nested grid and used as the observation operator in CarbonTracker. In TM5, atmospheric CO_2 concentrations are calculated using meteorological forecast fields from the European Centre for Medium Weather Forecast (ECMWF).

b. Ensemble Kalman filter

In CarbonTracker, the scaling factor is optimized through the ensemble square root filter (EnSRF) (Whitaker and Hamill, 2002), which is a type of EnKF (Evensen, 1994). Detailed description about EnKF data assimilation process in CarbonTracker can be found in previous studies (e.g., Peters et al., 2005; Kim et al., 2012, 2014a, 2014b, 2017).

Because the observation density is sparse and the released/absorbed surface CO_2 cannot be immediately transported to the atmosphere, it takes time to transmit the surface CO_2 flux signal at each grid point to the global observation sites. Therefore, the state vector optimized at the analysis step includes information from the previous and current states by adopting a smoother window (lag of weeks) in data assimilation. The assimilation window length in the current CarbonTracker is set to 5 weeks following the setting for North America (Peters et al., 2007). Robust surface CO_2 flux can be obtained using the 5 weeks of lag in North America due to the dense observation sites, whereas the 5 weeks of assimilation lag may not be appropriate for Asia with its relatively sparse observation sites.

The ensemble size is set to 150 following the settings for

North America. The Kalman gain matrix which is a weighting factor for the model and observation information is calculated according to the ensemble members in the EnKF, and would theoretically be more accurate as the ensemble size increases. The ensemble size is constrained by limited computer resources. However, sampling error may occur due to the finite ensemble size, which results in reduced accuracy of the estimated fluxes as well as the estimated flux uncertainty and makes the filter sensitive to observational data density. This problem could be improved by applying the covariance localization method or inflating the background error covariance (Houtekamer and Mitchell, 1998; Hamill et al., 2001). Because the physical distance between the scaling factors cannot be defined, Student's t-test with a 95% significance level is conducted to verify the significance of the calculated correlations between the ensemble of the scaling factor and the ensemble of the model CO_2 concentration. The covariance localization method is applied by setting the Kalman gain for the corresponding scaling factor to zero if the calculated correlations are not significant. The covariance localization is not applied for the Marine Boundary Layer (MBL) because observations in the MBL region are regarded to include flux information from remote regions as well as local regions (Peters et al., 2005). With this covariance localization method, 150 ensemble members were determined to be appropriate for North America and Europe (Peters et al., 2007). However, the optimum number of ensembles with covariance localization has not been investigated for the Asian region.

c. Observations

The measurement network of CO_2 observations used in this study is shown in Fig. 1. Observations are from NOAA (Conway et al., 2011; Andrews et al., 2014), Commonwealth Scientific and Industrial Research Organization (CSIRO, Langenfelds et al., 2002), Environment Canada (EC, Worthy et al., 2003), National Center for Atmospheric Research (NCAR, Stephens et al., 2011), Lawrence Berkeley National Laboratory (LBNL, Biraud et al., 2013), Instituto de Pesquisas Energeticas e Nucleares (IPEN, Gatti et al., 2010) (observation data is available at http://www.esrl.noaa.gov/gmd/ccgg/obspack/data.php; Masarie et al., 2014), Japan Meteorological Agency (JMA, Tsutsumi et al., 2006), World Data Centre for Greenhouse Gases (WDCGG, http://ds.data.jma.go.jp/wdcgg/), and Global Environmental Database of Center for Global Environment Research (CGER) National Institute for Environmental Studies (NIES).

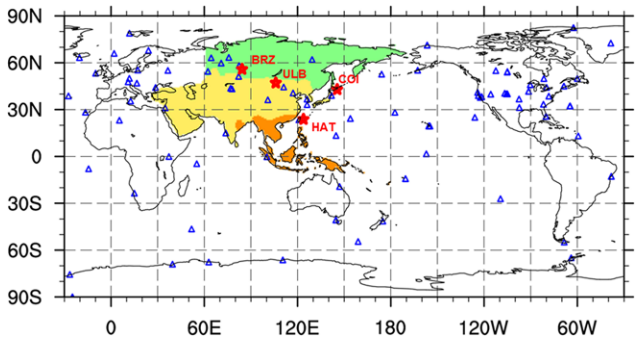

Fig. 1. Observation network of CO_2 concentrations over the globe. Each observation site is denoted by two colors: Blues are sites whose data are used in assimilation, whereas reds are sites whose data are not used in assimilation but used in verification. The EB, ET, and TA are denoted by green, yellow, and brown colors, respectively.

In addition to observations that are used in the previous CarbonTracker study of Kim et al., (2014b), observations in the Asian region are added for a more detailed analysis of surface CO_2 flux in Asia and verification of the results: surface CO_2 observations of Cape Rama (CRI, Bhattacharya et al., 2009), Gosan (GSN, Ju et al., 2007), LLN (Lulin, Sheu et al., 2009), and SDZ (Shangdianzi, Liu et al., 2009) distributed by WDCGG; Japan-Russia Siberian Tall Tower Inland Observation Network (JR-STATION) tower and aircraft measurements (Sasakawa et al., 2010, 2013), Cape Ochi-ichi (COI, Mukai et al., 2014a), and Hateruma island (HAT, Mukai et al., 2001, 2014b) distributed by CGER NIES. The observation sites for this study, including the newly added observation sites in the Asia region, are presented in Table 1.

Observations are averaged over 12-16 LST, 00-04 LST, or 14-18 LST according to the position and characteristics of each site. For example, sampling at night is valuable for observation sites located at high altitude because these sites are often affected by local valleys that are difficult to be accounted for in the model.

For validation, the optimized CO_2 concentrations are compared with observed CO_2 concentrations at Berezorechka (BRZ, aircraft only), Ulaanbaatar (ULB), COI, and HAT sites that are not used in data assimilation. Note that both the surface and aircraft observation data at BRZ are used in this study: the surface observation data at BRZ (hereafter BRZ_surf) is used in data assimilation and the aircraft observation data at BRZ (hereafter BRZ_air) is used for validation. The surface observations at COI and HAT and the BRZ_air are averaged over 12-16 LST for a more accurate comparison because the transport model is expected to characterize the well-mixed boundary layer better during the day than during the night (Peters et al., 2010). However, aircraft observations at ULB were used without filtering because they were mostly obtained in the morning. The aircraft observations at BRZ_air and ULB were sampled at from the planetary boundary layer to the lower free troposphere (up to few km). In addition, CO_2 measurements from Comprehensive Observation Network for Trace gases by Airliner (CONTRAIL) project were used to validate the modeled results. The CONTRAIL project was started in late 2005 to measure greenhouse gases using commercial airlines (Machida et al., 2008). The observation data from the CONTRAIL project have been used for verifying inverse modeling results (e.g., Feng et al., 2011; Houweling et al., 2015, Kim et al., 2016; Thompson et al., 2016).

Table 1. Observation sites located in Asia. MDM denotes Model-Data Mismatch. Note that observations in BRZ_air, ULB (aircraft), COI, and HAT are not used in assimilation but used for verification.

Region	Site Code	Latitude	Longitude	Height [m]	Laboratory	MDM [ppm]	Type
Eurasian Boreal	BRZ_surf	56.15°N	84.33°E	168	NIES	3	Continuous
	KRS	58.25°N	82.42°E	76	NIES	3	Continuous
	IGR	63.19°N	64.41°E	9	NIES	3	Continuous
	NOY	63.43°N	75.78°E	108	NIES	3	Continuous
	DEM	59.79°N	70.87°E	63	NIES	3	Continuous
	SVV	51.33°N	82.13°E	495	NIES	3	Continuous
	AZV	54.71°N	73.03°E	110	NIES	3	Continuous
	VGN	54.50°N	62.32°E	192	NIES	3	Continuous
	YAK	62.09°N	129.36°E	264	NIES	3	Continuous
	BRZ_air	56.15°N	84.33°E	vary	NIES	-	Aircraft
	ULB	47.40°N	106.20°E	vary	ESRL	-	Aircraft
Eurasian Temperate	WLG	36.29°N	100.90°E	3810	CMA/ESRL	1.5	Discrete
	WIS	31.13°N	34.88°E	400	ESRL	2.5	Discrete
	KZD	44.45°N	77.57°E	412	ESRL	2.5	Discrete
	KZM	43.25°N	77.88°E	2519	ESRL	2.5	Discrete
	TAP	36.73°N	126.13°E	20	ESRL	5	Discrete
	SDZ	40.39°N	117.07°E	287	CMA/ESRL	3	Discrete
	LLN	23.47°N	120.87°E	2862	ESRL	7.5	Discrete
	UUM	44.45°N	111.11°E	914	ESRL	2.5	Discrete
	CRI	15.08°N	73.83°E	60	CSIRO	3	Discrete
	MNM	24.29°N	153.98°E	8	JMA	3	Continuous
	RYO	39.03°N	141.82°E	260	JMA	3	Continuous
	YON	24.47°N	123.02°E	30	JMA	3	Continuous
	GSN	33.15°N	126.12°E	72	NIER	3	Continuous
	COI	43.16°N	145.50°E	94	NIES	-	Continuous
	HAT	24.06°N	123.81°E	47	NIES	-	Continuous
Tropical Asia	BKT	0.20°S	100.31°E	864	ESRL	7.5	Discrete

d. Experimental framework

By performing an Observing System Simulation Experiment (OSSE), Peters et al. (2005) showed that a 9-week assimilation window and 200 ensembles are appropriate for estimating the surface CO_2 flux using System for Ensemble Assimilation of Tracers in the Atmosphere (SEAT-A), which is the previous version of CarbonTracker. Peters et al. (2007) used a 5-week assimilation window and 150 ensembles in North America and Europe, where observations are distributed densely, and conducted a sensitivity test for 3-week and 10-week assimilation windows and 300 ensembles to assess a range of estimated surface CO_2 fluxes. Preceding studies for Asia have used a 5-week assimilation window and 150 ensembles (Peters et al., 2010; Kim et al., 2012, 2014a, 2014b; Zhang et al., 2014a, 2014b), the same settings used by Peters et al. (2007). Because the spatial distribution of observation sites in Asia is not as dense as in North America and Europe, a longer assimilation window length may be required for the Asia region, as observed in Peters et al. (2007). Babenhauserheide et al. (2015) showed that the carbon sink in Asia was increased by extending the assimilation window length from 5 to 10 weeks, whereas no further increase occurred from 10 to 15 weeks. Chatterjee et al. (2013) showed that inversion results become better by enlarging the ensemble size.

Experiments were set by considering computational costs as well as results from previous studies. Assimilation window lengths of 3, 5, 7, and 10 weeks and ensemble sizes of 100, 150, and 300 were tested. By combining the settings of assimilation window length and ensemble size, a total of 12 experiments were conducted (Table 2).

The TM5 transport model uses a 2-way nested grid. Kim et al. (2014a) showed that more detailed flux patterns for Asia can be obtained with a nested domain centered in East Asia. Accordingly, the nested domain centered in East Asia was applied with a $3^\circ \times 2^\circ$ horizontal resolution in the globe and $1^\circ \times 1^\circ$ (latitude 12°S-54°N, longitude 66°E-153°E) horizontal resolution in East Asia.

Table 2. Experimental name of sensitivity tests for the number of ensemble and assimilation window length.

Experimental Settings		Ensemble size		
		100	150	300
Assimilation window length	3	L3E100	L3E150	L3E300
	5	L5E100	L5E150	L5E300
	7	L7E100	L7E150	L7E300
	10	L10E100	L10E150	L10E300

The optimized surface CO_2 flux in the Asia region was analyzed with a classification of EB, ET, and TA in the Transcom region (Gurney et al., 2002). A total of 22 regions in Transcom are composed of 11 land and 11 ocean regions. Fire and fossil fuel fluxes were excluded from the analysis because they use prior fluxes intact. The experimental period was from 1 January, 2006, to 31 December, 2009, and the first year was regarded as a spin-up period and excluded from the analysis period.

3. Results

a. Surface CO_2 flux

Figure 2 represents the distribution of the prior and posterior (i.e., optimized) biosphere fluxes of L5E150 (i.e., current configuration of CarbonTracker) in Asia averaged over 2007-2009. Before optimization, the magnitudes of absorption and emission of surface CO_2 flux in Asia are quite small (Fig. 2a). After optimization, the regional difference in surface CO_2 flux becomes distinct in the Asia region (Fig. 2b). In Asia, most regions show carbon absorptions except the Indian subcontinent, parts of Indonesia, and northern Taiga of the EB region. Net carbon exchange between land/ocean and atmosphere in Asia estimated using L5E150 configuration was -1.09 ± 0.69 PgC yr^{-1} (the range was -1.19 - -0.97 PgC yr^{-1} among all experiments in this study). Negative sign means carbon absorption by the surface, whereas positive sign implies carbon emission to the atmosphere from the surface. The estimated carbon absorption in Asia in this study was smaller than other inversion studies using CarbonTracker such as CarbonTracker 2015 (CT2015; -1.92 ± 4.32 PgC yr^{-1} for 2007-2009), CarbonTracker-Europe 2015 (CTE2015; -1.65 ± 0.82 PgC yr^{-1} for 2007-2009), and CTDAS (CarbonTracker Data Assimilation System) with CONTRAIL data (Zhang et al. 2014b, -1.56 ± 1.34 PgC yr^{-1} for 2006-2010), which may be caused by additionally assimilated Siberian observations (Kim et al., 2017). As in other studies, the intensity of absorption was largest in the EB region, where carbon uptake primarily occurred, followed by the ET region except for the desert and Indian region. The intensity of flux in the TA region is weaker compared with that in the EB and ET regions. Although the regional division and the experimental period were slightly different, the estimated carbon absorption in this study was comparable to that (-1.05 ± 0.43 PgC yr^{-1} for 2001-2004) in Peylin et al. (2013), for the North Asian region (roughly corresponding to EB and ET in this study).

Differences between the optimized biosphere fluxes of L5E150 and other experiments are presented in Fig. 3. For the 150 ensemble experiments (Figs. 3b, e, h, and k), carbon sinks increase when the assimilation window length becomes longer. For the 100 and 300 ensemble experiments, changes in fluxes are more distinct in the EB regions compared to the ET regions (e.g., compare Figs. 3c and f). For all assimilation window length experiments, the overall and regional fluxes change distinctly as the ensemble size becomes larger. The carbon sinks decreased in the EB and China in the ET but increased in the Indian subcontinent in the ET (compare Figs. 3d and f). Thus, both ensemble size and assimilation window length

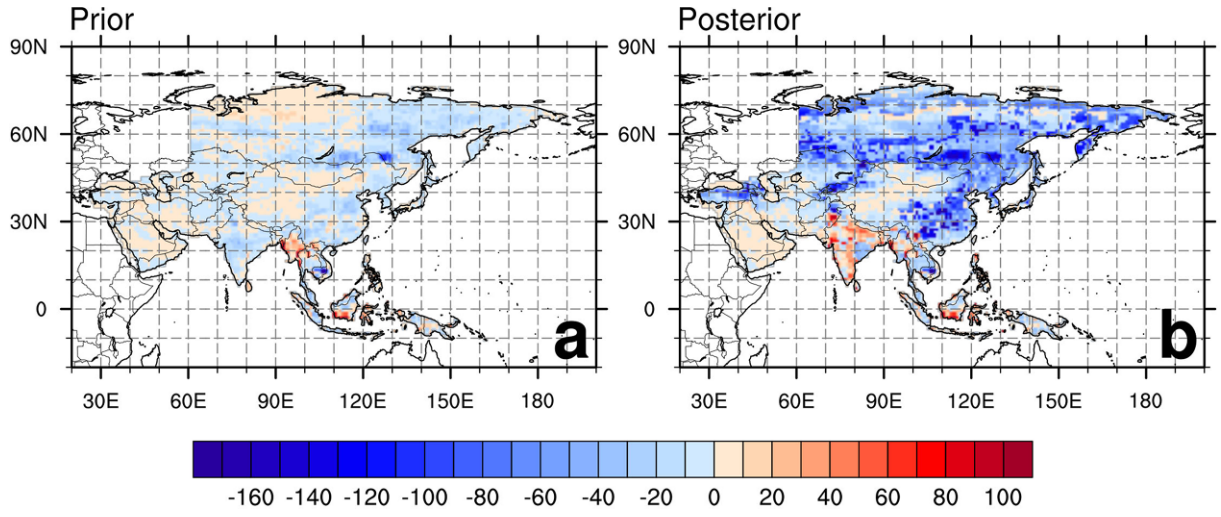

Fig. 2. (a) Prior and (b) posterior (i.e., optimized) biosphere fluxes (g C m^{-2} yr^{-1}) of L5E150 in Asia averaged over 2007-2009. Blue color denotes net carbon uptake by the surface whereas red color denotes carbon release to the atmosphere.

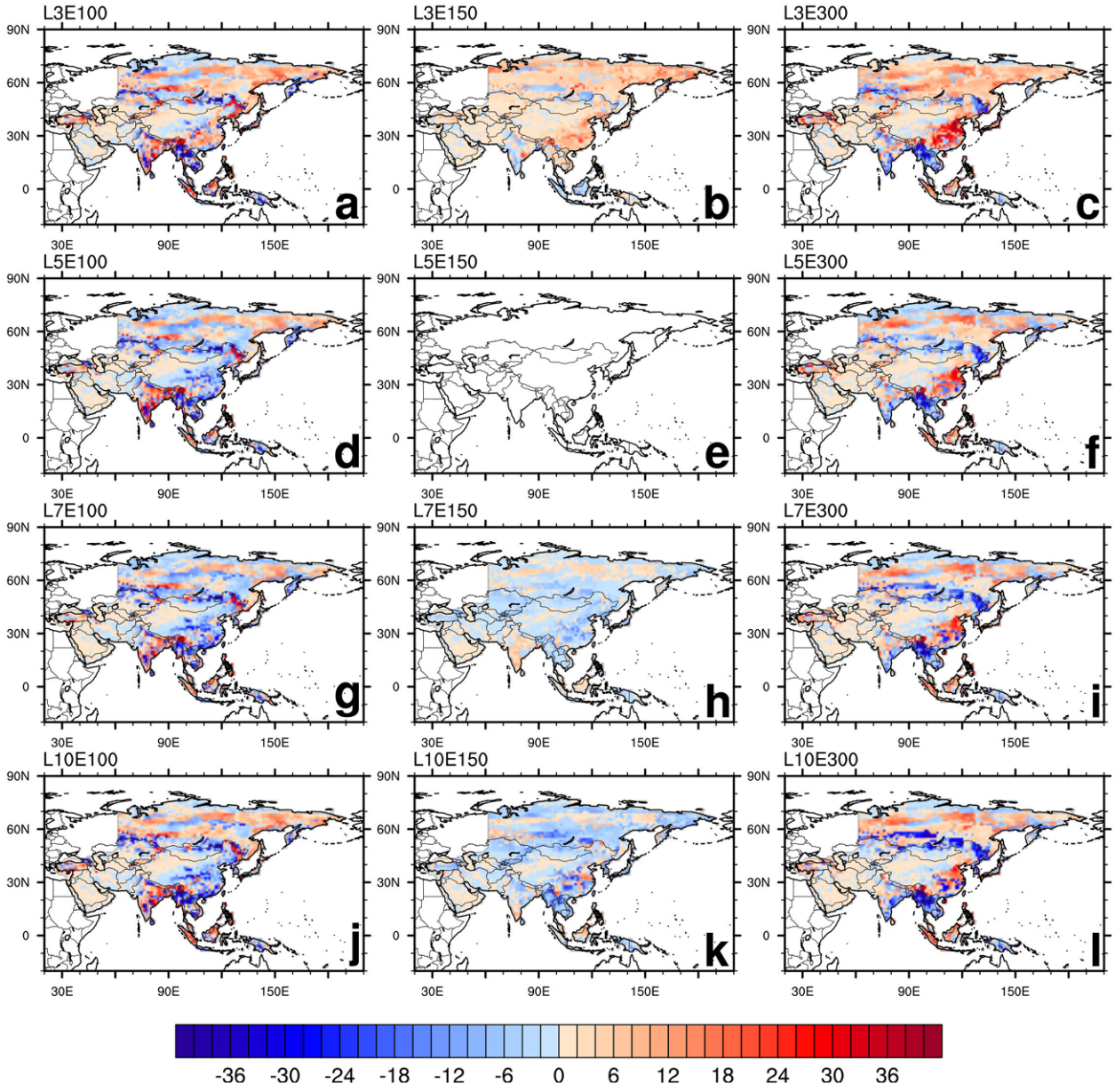

Fig. 3. The difference of the optimized biosphere fluxes (g C m^{-2} yr^{-1}) of (a) L3E100, (b) L3E150, (c) L3E300, (d) L5E100, (e) L5E150, (f) L5E300, (g) L7E100, (h) L7E150, (i) L7E300, (j) L10E100, (k) L10E150, and (l) L10E300 from the optimized biosphere fluxes of L5E150, averaged over 2007-2009 in Asia. Note that (e) is an empty field because the differences are calculated based on L5E150.

affect the flux distribution of the carbon absorption and emission in Asia, but the flux distribution shows more distinct features according to the ensemble size, which implies that the overall effect of ensemble size on the surface CO_2 flux distribution is larger compared to that of the assimilation window length.

To assess the sensitivity of regional distribution due to experimental configuration, the standard deviation of the optimized surface CO_2 fluxes of the experiments in summer (JJA) and winter (DJF) for the Asian region is shown in Fig. 4. Differences between the optimized surface CO_2 fluxes of the experiments are greater in summer than winter. The greatest differences exist in EB, followed by ET and TA, which implies that the absorption and emission of surface CO_2 fluxes in EB are sensitive to experimental settings in summer because the absorption and emission in EB are more active in summer compared to those in other regions or seasons in addition to the seasonal change of the atmospheric transport.

Annual biosphere and ocean fluxes for each Transcom region and the globe are presented in Table 3. For global fluxes, the carbon sink of the prior flux in land is smaller than that of the posterior flux, whereas the carbon sink of the prior

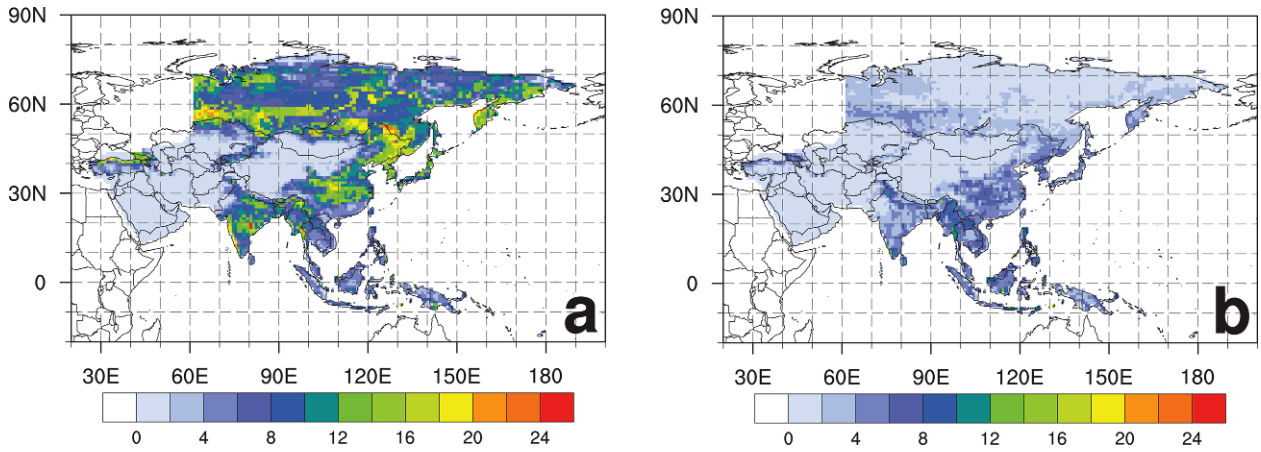

Fig. 4. The standard deviation of the optimized surface biosphere fluxes (g C m^{-2} yr^{-1}) between 12 experiments of (a) JJA and (b) DJF averaged over 2007-2009.

Table 3. Annual optimized biosphere and ocean fluxes (Pg C yr^{-1}) averaged over 2007-2009 for each Transcom region in Asia and the globe for each experiment.

Region Name	Prior	L3E100	L5E100	L7E100	L10E100
Eurasia Boreal	−0.08	−0.63	−0.66	−0.68	−0.64
Eurasia Temperate	−0.07	−0.39	−0.44	−0.46	−0.46
Tropical Asia	0.02	−0.03	−0.03	−0.02	−0.03
Global	−4.15	−5.29	−5.60	−5.74	−5.80
Land	−1.34	−3.64	−3.81	−3.88	−3.92
Ocean	−2.81	−1.65	−1.79	−1.86	−1.88
Region Name	Prior	L3E150	L5E150	L7E150	L10E150
Eurasia Boreal	−0.08	−0.59	−0.65	−0.66	−0.68
Eurasia Temperate	−0.07	−0.40	−0.44	−0.46	−0.47
Tropical Asia	0.02	0.00	−0.01	−0.02	−0.03
Global	−4.15	−5.38	−5.64	−5.78	−5.85
Land	−1.34	−3.60	−3.76	−3.86	−3.93
Ocean	−2.81	−1.78	−1.88	−1.92	−1.92
Region Name	Prior	L3E300	L5E300	L7E300	L10E300
Eurasia Boreal	−0.08	−0.60	−0.65	−0.66	−0.66
Eurasia Temperate	−0.07	−0.35	−0.39	−0.41	−0.43
Tropical Asia	0.02	−0.02	−0.02	−0.03	−0.04
Global	−4.15	−5.46	−5.70	−5.81	−5.88
Land	−1.34	−3.68	−3.83	−3.92	−3.95
Ocean	−2.81	−1.77	−1.87	−1.89	−1.92

flux in ocean is greater than that of the posterior flux. Total carbon uptakes increase after optimization. The EB, ET, and TA in Asia are sink regions of surface CO_2 fluxes (Pan et al., 2011). Differences between prior and posterior surface CO_2 flux and between experiments are greater for the EB and ET than for other regions. The magnitude of flux differences and flux itself are small in the TA.

The uptakes of average optimized surface CO_2 fluxes for the globe over 2007-2009 increase as the assimilation window length becomes longer and the ensemble size becomes larger (Fig. 5a). The uptakes of average optimized surface CO_2 fluxes in Asia increase as the assimilation window length increases, except L10E100, but decrease as the ensemble size increases (Fig. 5b), which is different from the global fluxes and more distinctly shown in ET than EB. The increase of the uptake of average optimized surface CO_2 fluxes for longer assimilation

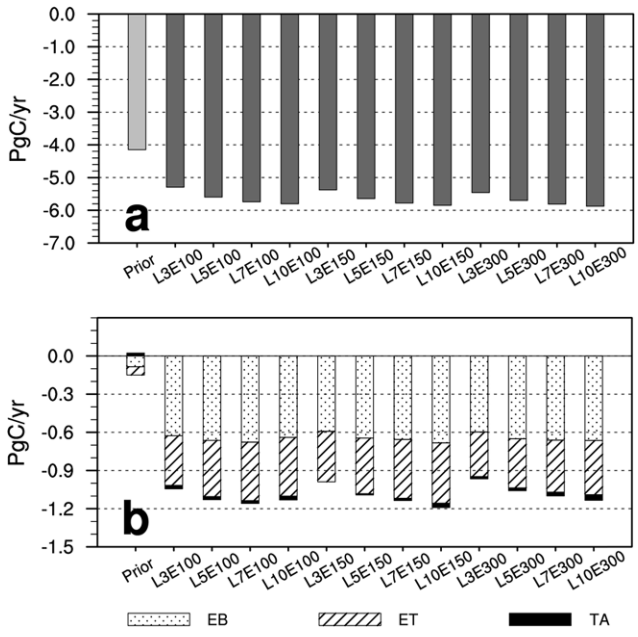

Fig. 5. Annual optimized biosphere and ocean fluxes (Pg C yr^{-1}) averaged over 2007-2009 for (a) the globe and (b) each Transcom region in Asia (i.e., EB, ET, and TA) for each experiment. In (a), light gray represents the prior flux and dark gray represents the posterior flux over globe.

window length is consistent with the results in Babenhauseheide et al. (2015).

Figure 6 presents the optimized biosphere fluxes that are weekly cumulated for EB, ET, and TA averaged over 2007-2009. The differences between experiments become greater after the summer, which implies that the absorption of vegetation in summer has a large impact on the results of each experiment. The intensity of absorption and emission of surface CO_2 flux is strong in EB compared to other regions. The intensity of absorption in EB increases as the assimilation window length becomes longer, which implies that the intensity of absorption is more sensitive to the assimilation window length than the ensemble size (Figs. 6a and d). The effect of the assimilation window length is important for EB because the distribution of vegetation and weather phenomena in EB are relatively simple and there are sparse observation sites. In contrast, the intensity of absorption and emission of surface CO_2 fluxes in ET is sensitive to both the ensemble size and the assimilation window length (Figs. 6b and e) due to the complex distribution of vegetation and various weather phenomena in ET. Differences between experiments in TA are less than those in EB and ET (Figs. 6c and f) because data assimilation is not highly effective in TA due to the small intensity of surface CO_2 flux and few observations in TA compared to EB and ET. Therefore, additional observations are required to optimize the surface CO_2 flux in TA rather than the optimization of assimilation parameters.

Overall, the averaged absorption intensity and difference in averaged intensity of optimized biosphere fluxes among experiments are largest in EB, followed by ET and TA. In Asia, as the assimilation window length increases, the uptake of optimized biosphere fluxes increases. In contrast, as the ensemble size increases, the uptake decreases. Although the effect of ensemble size on the distribution of surface CO_2 flux in Asia is generally larger than the effect of the assimilation window length in Asia, the importance of the assimilation window length and ensemble size on the distribution of surface CO_2 flux varies in specific regions in Asia.

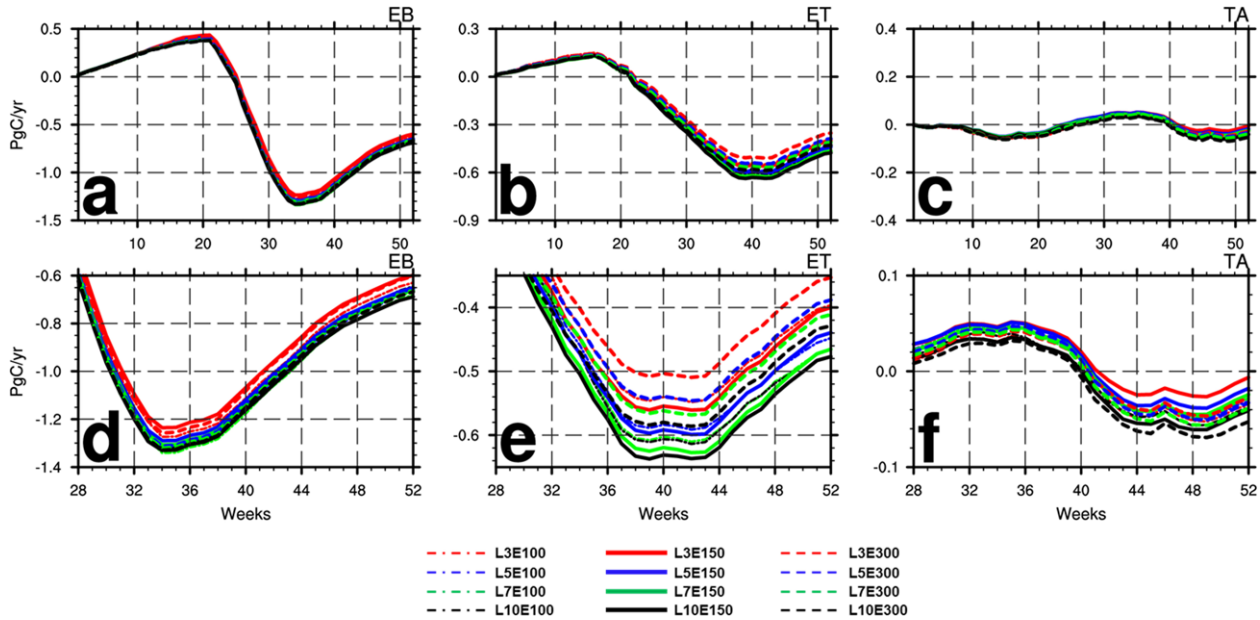

Fig. 6. Weekly cumulative flux in: (a) EB, (b) ET, (c) TA region averaged over 2007-2009. (d), (e), and (f) are the magnifications of (a), (b), and (c) in the latter part of year, respectively. Note that EB, ET, and TA region use different scales in y-axis.

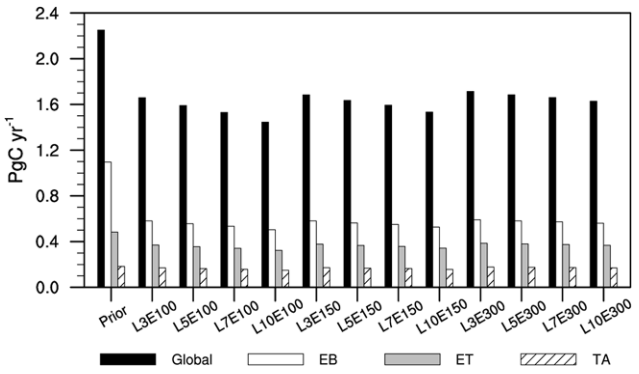

Fig. 7. Histogram of prior and posterior uncertainty (Pg C yr^{-1}) in the globe (black), EB (white), ET (grey), and TA (slash) region for each experiment averaged over 2007-2009.

b. Uncertainty (ensemble spread) associated with surface CO_2 flux

Figure 7 presents the uncertainty of optimized surface CO_2 fluxes for each experiment in the globe, EB, ET, and TA. The uncertainty is obtained by a standard deviation of optimized surface CO_2 fluxes. The overall uncertainty was reduced through the optimization process by 24-36% in the globe and 46-54%, 20-33%, 1-17% over EB, ET, and TA, respectively, for all experiments. EB shows the largest uncertainty reduction after optimization. TA shows the smallest differences between prior and posterior uncertainties, which reaffirms the slight data assimilation effect for TA. The uncertainty of global flux is reduced as the assimilation window length becomes longer, and the increase in the reduction rate due to the assimilation window length is distinct for smaller ensemble experiments. In contrast, the uncertainty of global flux increases as the ensemble size becomes larger. The uncertainties of regional (i.e., EB, ET, TA) fluxes show a similar decreasing (increasing) trend as the assimilation window length (ensemble size) increases. Detailed values are shown in Table 4.

To illustrate the regional distribution of reduced uncertainties after optimization, the uncertainty reduction (UR) of L5E150 for the Asian region is shown in Fig. 8. UR is calculated as in Eq. (2) similar to previous studies (Peters et al., 2005; Meirink et al., 2008; Chevallier et al., 2009; Feng et al., 2009):

$$\mathrm{UR} = \left(1 - \frac{posterior\ uncertainty}{prior\ uncertainty}\right) \times 100 \quad (2)$$

where prior uncertainty denotes the uncertainty of prior fluxes and posterior uncertainty denotes the uncertainty of optimized fluxes, calculated using the standard deviation of ensembles for each scaling factor in each grid point. The UR is largest in EB, followed by ET (Fig. 8), consistent with Fig. 7.

The differences in UR between other experiments and L5E150 are presented in Fig. 9. Compared to the UR of L5E150, the URs of other experiments become large as the ensemble size becomes smaller and the assimilation window length becomes longer. As the assimilation window becomes longer, more observations are assimilated and the posterior

Table 4. Prior and posterior uncertainty (Pg C yr^{-1}) in EB, ET, TA and globe averaged over 2007-2009.

Region Name	Prior	L3E100	L5E100	L7E100	L10E100
Eurasia Boreal	1.10	0.58	0.56	0.53	0.50
Eurasia Temperate	0.48	0.37	0.36	0.34	0.32
Tropical Asia	0.18	0.17	0.16	0.16	0.15
Global	2.25	1.66	1.59	1.53	1.45
Land	1.88	1.32	1.27	1.22	1.15
Ocean	1.24	1.00	0.96	0.93	0.88
Region Name	Prior	L3E150	L5E150	L7E150	L10E150
Eurasia Boreal	1.10	0.58	0.56	0.55	0.53
Eurasia Temperate	0.48	0.38	0.37	0.36	0.34
Tropical Asia	0.18	0.17	0.17	0.16	0.16
Global	2.25	1.68	1.63	1.59	1.53
Land	1.88	1.34	1.30	1.27	1.22
Ocean	1.24	1.02	0.99	0.97	0.93
Region Name	Prior	L3E300	L5E300	L7E300	L10E300
Eurasia Boreal	1.10	0.59	0.58	0.57	0.56
Eurasia Temperate	0.48	0.39	0.38	0.37	0.37
Tropical Asia	0.18	0.18	0.17	0.17	0.17
Global	2.25	1.71	1.68	1.66	1.63
Land	1.88	1.37	1.34	1.32	1.30
Ocean	1.24	1.03	1.02	1.00	0.98

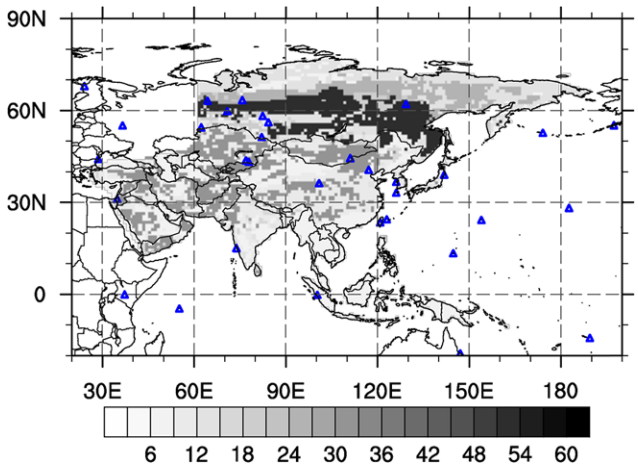

Fig. 8. Uncertainty reduction (%) of L5E150 averaged over 2007-2009 with the measurement sites (blue).

uncertainty becomes smaller, which implies large uncertainty reduction. In contrast, smaller ensembles have less ensemble spread, leading to artificial reduction of a posterior uncertainty, which results in large uncertainty reduction. Thus, the large uncertainty reduction by the smaller ensembles may include the sampling error. In comparison with the existing L5E150 configuration, the UR of L10E100 is the largest (Fig. 9j) and the UR of L10E300 is similar to that of L5E150 with more regional variations (Fig. 9l). Symmetrical patterns between L7E100 and L10E150 imply that reduced uncertainties accompanying a longer assimilation window (Fig. 9g) can be compensated for by larger uncertainties with a larger ensemble size (Fig. 9k).

Overall, as the assimilation window length increases, the uncertainty of optimized biosphere fluxes decreases and UR increases. In contrast, as the ensemble size increases, the uncertainty increases and UR decreases.

c. Verification

(1) Growth rate

To verify the validity of the inversion results, the growth rate (GR) of the atmospheric CO_2 concentration estimated from the model has been compared to that from the observations (e.g., Rayner et al., 2005; Bruhwiler et al., 2011). To assess the balance of the carbon absorption and emission in the globe, the GR of the global atmospheric CO_2 concentrations estimated from each experiment is compared to that of the observed CO_2 concentration provided by NOAA (www.esrl.noaa.gov/gmd/ccgg/trends/global.html). The GR provided by NOAA is the annual mean global GR (i.e., the total sum of CO_2 that emitted to and removed from the atmosphere globally during a year) inferred directly from the observed CO_2 concentrations at marine surface sites. In contrast, the GR of the global atmospheric CO_2 concentration estimated in each experiment is calculated from total annual global flux estimated from each experiment as:

$$\mathrm{GR} = (\textit{Total flux}) \times (\textit{Conversion factor}) \quad (3)$$

where total flux is the sum of the global biosphere, ocean, fire, and fossil fuel fluxes, and the conversion factor is 0.47 ppm $(\mathrm{Pg\ C})^{-1}$ (e.g., Fujii, 1990; Battle et al., 2000). The conversion

Table 5. RMSE, bias, and standard deviation of the bias (ppm), averaged over 2007-2009.

NAME	L3E100			L5E100			L7E100			L10E100		
	RMSE	BIAS	STD	RMSE	BIAS	STD	RMSE	BIAS	STD	RMSE	BIAS	STD
ULB	1.75	0.18	1.75	1.67	0.2	1.66	1.6	0.18	1.59	1.58	0.17	1.57
BRZ_air	2.94	–0.38	2.92	2.96	–0.38	2.93	2.92	–0.39	2.9	2.87	–0.37	2.84
COI	4.17	1.46	3.9	4.19	1.41	3.94	4.17	1.39	3.93	4.16	1.4	3.92
HAT	2.4	0.29	2.38	2.37	0.34	2.34	2.35	0.33	2.32	2.35	0.32	2.33
NAME	L3E150			L5E150			L7E150			L10E150		
	RMSE	BIAS	STD	RMSE	BIAS	STD	RMSE	BIAS	STD	RMSE	BIAS	STD
ULB	1.84	0.37	1.81	1.8	0.34	1.77	1.81	0.3	1.79	1.79	0.23	1.78
BRZ_air	2.83	–0.23	2.82	2.79	–0.36	2.76	2.8	–0.4	2.77	2.84	–0.39	2.81
COI	4.05	1.49	3.77	4.09	1.36	3.86	4.17	1.32	3.96	4.2	1.27	4.01
HAT	2.43	0.48	2.38	2.4	0.44	2.36	2.39	0.41	2.36	2.37	0.36	2.35
NAME	L3E300			L5E300			L7E300			L10E300		
	RMSE	BIAS	STD	RMSE	BIAS	STD	RMSE	BIAS	STD	RMSE	BIAS	STD
ULB	1.74	0.25	1.72	1.68	0.23	1.67	1.67	0.17	1.66	1.62	0.14	1.62
BRZ_air	2.78	–0.38	2.75	2.76	–0.38	2.73	2.75	–0.4	2.72	2.78	–0.44	2.74
COI	4.05	1.47	3.77	4.03	1.38	3.78	3.98	1.31	3.76	3.99	1.29	3.78
HAT	2.4	0.35	2.37	2.38	0.36	2.35	2.37	0.33	2.35	2.36	0.3	2.34

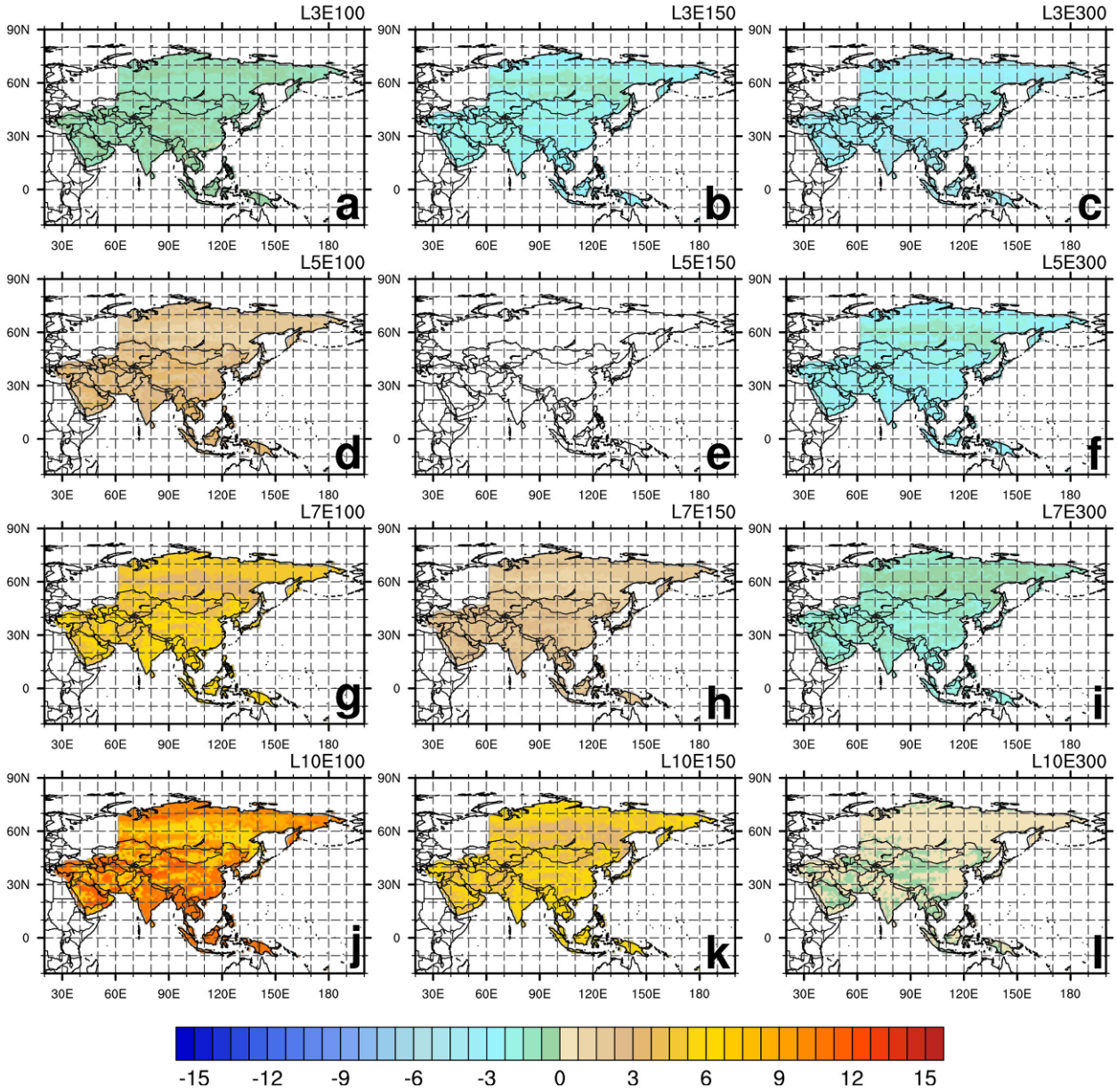

Fig. 9. The difference of uncertainty reduction (%) of (a) L3E100, (b) L3E150, (c) L3E300, (d) L5E100, (e) L5E150, (f) L5E300, (g) L7E100, (h) L7E150, (i) L7E300, (j) L10E100, (k) L10E150, (l) L10E300 from L5E150, respectively, averaged over 2007-2009. Note that (e) is an empty field because the differences are calculated based on L5E150.

factor is used to convert the optimized CO_2 flux (Pg C) to CO_2 concentration (ppm) in each experiment.

Table 6 shows the GR of the atmospheric CO_2 concentrations (ppm) during 2007-2009. The GR estimated from the prior CO_2 flux is generally greater than that estimated from the optimized CO_2 flux. As the assimilation window length becomes longer and the ensemble size becomes larger, the GR estimated from the optimized CO_2 flux becomes closer to that of the observed CO_2 concentration. This tendency is consistent with the previous result in Fig. 5, which shows increasing carbon absorption with longer assimilation window length and larger ensemble size. Estimation of more CO_2 absorption in biosphere and land for longer assimilation window length and larger ensemble size offsets the fossil fuel emission, which leads the reduced GR closer to observations. As a result, the L10E300 experiment shows the GR closest to that of observations.

(2) Verification using assimilated observations

To verify the modeled CO_2 concentrations, the modeled CO_2 were compared with the observations that used for data assimilation (22 sites located in Asia, Table 1). Figure 10 shows the bias and RMSE/MDM between modeled and observed CO_2 concentrations. Except for L10E100, bias decrease as the

Table 6. Growth rate (GR) of atmospheric CO_2 concentrations [ppm] for each experiment during 2007-2009. The observed GR is obtained from NOAA which is inferred directly from the observed CO_2 at marine surface sites.

GR	prior	L3E100	L5E100	L7E100	L10E100	obs.
2007	2.99	3.00	2.85	2.76	2.66	2.09
2008	2.88	2.08	1.94	1.90	1.91	1.78
2009	2.58	1.76	1.61	1.55	1.55	1.62
avg	2.82	2.28	2.14	2.07	2.04	1.83
GR	prior	L3E150	L5E150	L7E150	L10E150	obs.
2007	2.99	3.05	2.81	2.71	2.59	2.09
2008	2.88	1.94	1.89	1.84	1.89	1.78
2009	2.58	1.74	1.65	1.62	1.57	1.62
avg	2.82	2.24	2.11	2.05	2.02	1.83
GR	prior	L3E300	L5E300	L7E300	L10E300	obs.
2007	2.99	2.97	2.79	2.65	2.56	2.09
2008	2.88	1.95	1.83	1.83	1.81	1.78
2009	2.58	1.69	1.64	1.64	1.64	1.62
avg	2.82	2.20	2.09	2.04	2.01	1.83

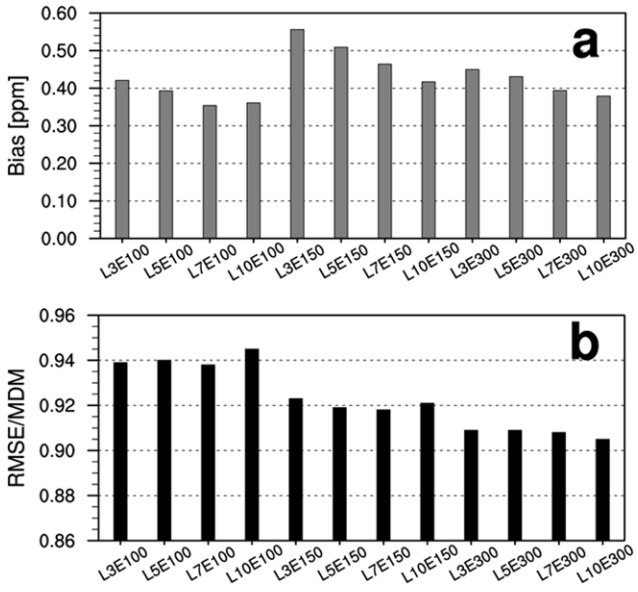

Fig. 10. (a) Bias [ppm] and (b) RMSE/MDM between modeled CO_2 concentrations and observed CO_2 concentrations of each experiment in 22 observation sites in Asia, whose data are used in assimilation.

assimilation window length becomes longer for the experiments with the same ensemble size (Fig. 10a). More observations can be assimilated for longer assimilation window length, which leads smaller bias. The RMSE/MDM decreases as the ensemble size increases, whereas it does not vary depending on the assimilation window length for the experiments with the same ensemble size (Fig. 10b). The RMSE/MDM of L10E300 is the smallest, showing a decreased

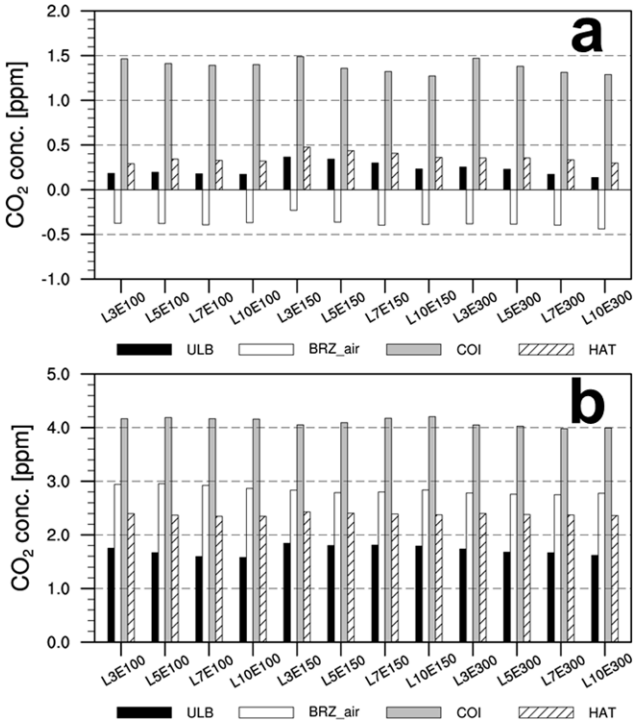

Fig. 11. (a) Bias [ppm] and (b) RMSE [ppm] between modeled CO_2 concentrations and observed CO_2 concentrations of each experiment in 4 independent observation sites (ULB, BRZ_air, COI, and HAT).

RMSE/MDM with a larger ensemble size for the experiments with the same assimilation window length (Fig. 10b). For the small ensemble size (i.e., 100), bias and RMSE increase slightly with the longest assimilation window length (i.e., 10 weeks), which may be caused by the filter divergence of EnKF.

(3) Verification using independent observations from 4 observation sites

The simulated CO_2 concentrations of each experiment were compared with independently observed CO_2 concentrations that were not used in data assimilation. Observations used in verification were from 4 observation sites: COI, HAT, BRZ_air, and ULB. Observations in COI and HAT are surface measurements, and observations in BRZ_air and ULB are aircraft measurements (Table 1).

The bias and RMSE between the simulated CO_2 concentrations and the observed CO_2 concentrations at 4 observation sites are presented in Fig. 11. The bias varies depending on the observation sites, showing a negative bias in BRZ_air and positive bias in other sites (Fig. 11a). Note that the magnitudes of the bias and RMSE at COI are much larger compared to those at other sites. The COI is a coastal site under the influence of both land and ocean fluxes (Ballav et al., 2012), which is difficult to predict offshore and onshore flow accurately in the transport model (Law et al., 2008; Patra et al., 2008). Four experiments with 100 ensembles showed small differences in bias depending on the assimilation window

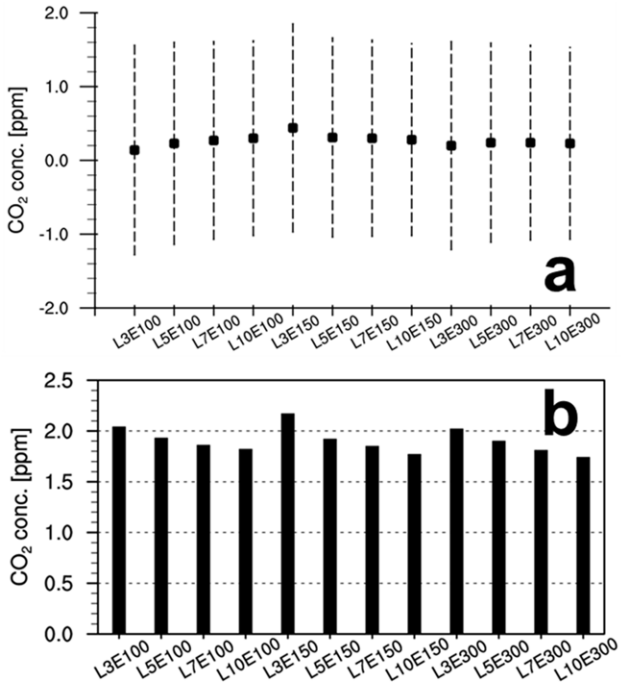

Fig. 12. (a) Average (black rectangle) and standard deviation (dotted bar) of bias [ppm] and (b) RMSE [ppm] between modeled CO_2 concentrations and observed CO_2 concentrations obtained from the CONTRAIL project. Observations above 625 hPa were used in analysis following Niwa et al. (2012).

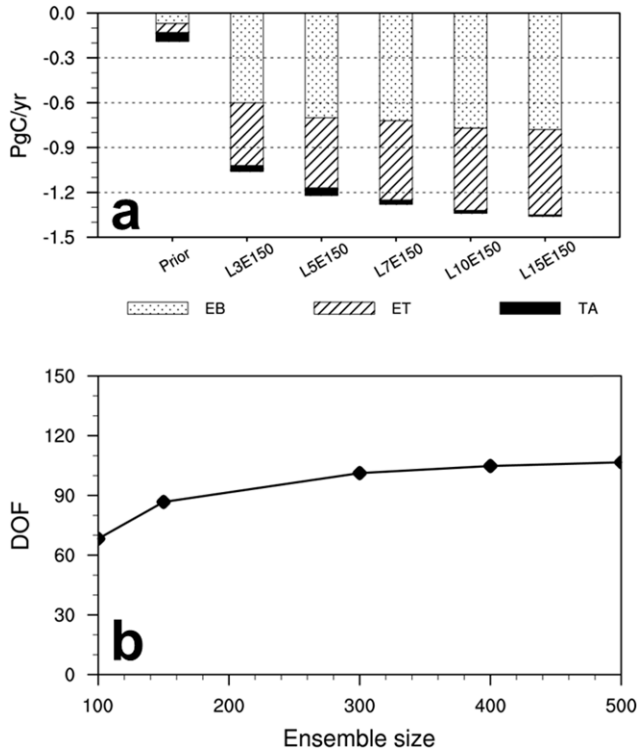

Fig. 13. (a) The optimized biosphere fluxes (Pg C yr^{-1}) of the experiments with 3, 5, 7, 10, and 15 weeks of assimilation window length for each Trancom region in Asia (i.e., EB, ET, and TA) during 2007 and (b) the number of degrees of freedom (DOF) as a function of ensemble size.

length, which implies that the assimilation window length does not affect the bias much for small ensembles. Except BRZ_air, for 150 and 300 ensembles, biases decrease as the assimilation window length becomes longer, showing the smaller biases for experiments with 10-week assimilation window (i.e., L10E150 and L10E300). In case of RMSE, although the results vary slightly among observation sites, on average, the RMSE of L10E300 is the smallest, showing a decreased RMSE with a larger ensemble size (Fig. 11b). For 300 ensemble experiments, the RMSE decreases with a longer assimilation window. Detailed values are shown in Table 5.

(4) Verification using independent observations from the CONTRAIL project

In addition to the independent CO_2 observations from 4 observation sites in Section 3.3.3, CO_2 measurements from the CONTRAIL project were used to validate the modeled results. Following Niwa et al. (2012), the observations above 625 hPa during 2007-2009 were used in analysis to exclude the effect of big cities near the airports at lower altitudes. Note that approximately half of vertical profile data are obtained over Tokyo because the CONTRAIL project is based on the measurements of Japan Airlines flights.

Figure 12 represents the average bias and RMSE between modeled CO_2 concentrations and observed CO_2 concentrations obtained from the CONTRAIL project. Although the average bias shows different tendencies depending on the ensemble size (Fig. 12a), the standard deviation of bias decreases as the assimilation window length increases for the same ensemble size, which implies that the longer assimilation window length reduces the variability of the bias. Except for L3E150, average RMSE decreases as the assimilation window length becomes longer and the ensemble size becomes larger (Fig. 12b).

Based on verifications using CO_2 observations, the configuration of a 10-week assimilation window and 300 ensembles is most suitable combination of data assimilation parameters for estimating surface CO_2 flux in the Asian region. The result for 10-week assimilation window is the best when the ensemble size is large (e.g., 300). Because observation sites are sparsely distributed in the Asian region, the longer assimilation window length is more appropriate when the number of ensembles is 300.

(5) Verification with larger ensemble size and longer assimilation window length

Additional experiments with even larger ensemble size (i.e., 400 and 500) and longer assimilation window length (i.e., 15 weeks) were implemented to check whether the ensemble size and assimilation window length tested in this study are appropriate to get sufficiently reliable flux estimates for the Asian region. The experimental period of the additional experiments was from 1 January, 2006, to 31 December, 2007, and the

results of 2007 were analyzed because 2006 was regarded as spin-up period.

In case of longer assimilation window length, the carbon sink in Asia increases as the assimilation window length becomes longer (Fig. 13a). However, the increasing slope becomes more gradual with longer assimilation window length, especially between 10 and 15 weeks of assimilation window length (Fig. 13a), which implies that the carbon sink of the biosphere flux in Asia reaches to a saturation point with 10 weeks of assimilation window length. In addition, increasing the number of ensembles shows a tendency of convergence after 300 based on the degrees of freedom (DOF) (Fig. 13b) which is a measure of how well the estimated covariance matrix captures the complete covariance structure. The DOF is calculated as in Eq. (4) following Patil et al. (2001) and Peters et al. (2005), for a randomly chosen week because the DOF varies very slightly from week to week:

$$\mathrm{DOF} = \frac{\left(\sum_{i=1}^{N} \omega_i\right)^2}{\sum_{i=1}^{N} \omega_i^2} \tag{4}$$

where ω_i denote the singular values obtained from a singular value decomposition of the analysis error covariance matrix and N is the number of ensembles. These results reaffirm that the 10-week assimilation window length and 300 ensembles are appropriate to estimate reliable surface CO_2 flux in the Asian region.

4. Conclusions

Sensitivity tests using several combinations of assimilation window length and ensemble size were conducted to identify the optimum set of data assimilation parameters in the current CarbonTracker for the Asian region. The assimilation window lengths used were 3, 5, 7, and 10 weeks, and the ensemble sizes used were 100, 150, and 300, resulting in a total of 12 experimental combinations. The experimental period was from January 1, 2006, to December 31, 2009, and 2006 was regarded as spin-up period and excluded from analysis. The results were analyzed in EB, ET, and TA in the Transcom region. The biosphere flux, which is the most important flux for the optimization of surface CO_2 flux in Asia, was mainly analyzed among biosphere, ocean, fire, and fossil fuel fluxes, which constitute the surface CO_2 fluxes.

The absorption intensity and difference in intensity of the optimized biosphere fluxes among the experiments were largest in EB, followed by ET and TA. In the globe, as the assimilation window length and ensemble size increase, the uptake of surface CO_2 flux increases. However, in Asia, as the assimilation window length increases, the uptake of optimized biosphere fluxes increases but the uncertainty of optimized biosphere fluxes decreases. In contrast, as the ensemble size increases, the uptake decreases and uncertainty increases. The optimized biosphere flux is more sensitive to assimilation window length in EB, whereas it is sensitive to ensemble size as well as the assimilation window length in ET. Because of the relatively simple distribution of vegetation and weather phenomena in EB, the assimilated observation number (associated with the assimilation window length) is important for optimization and uncertainty decreases after optimization due to the effect of assimilating observations. In contrast, the complex distribution of vegetation and various weather phenomena in ET causes the optimized biosphere flux to be sensitive to ensemble size, resulting in increased uncertainties. The difference between experiments is small in TA due to the small effect of data assimilation in TA. Overall, the optimized biosphere fluxes are more affected by ensemble size than assimilation window length and present more detailed distributions with 300 ensembles.

The results were verified using the growth rate of CO_2 at Mauna Loa, observed CO_2 concentrations from observation sites located in Asia, and observed CO_2 concentrations from the CONTRAIL project. The bias and RMSE of observed and simulated CO_2 concentrations for each observation site revealed that the configuration of a 10-week assimilation window length and 300 ensembles is most appropriate for the Asian region in the CarbonTracker framework. The simulated CO_2 concentrations produce the best results when the number of ensembles is 300. Further, the result for 10-week assimilation window is the best when the ensemble size is large (e.g., 300). Considering the sparse observation sites in the Asian region, the longer assimilation window length is more appropriate when the number of ensembles is large enough to represent uncertainties (i.e., 300). Additional experiments with even larger ensemble size (i.e., 400 and 500) and longer assimilation window length (i.e., 15 weeks) reaffirm that the 10-week assimilation window length and 300 ensembles are appropriate in optimizing surface CO_2 flux in the Asian region in CarbonTracker. The configuration of a 10-week assimilation window length and 300 ensembles is computationally expensive, nearly four times as expensive as the existing configuration of a 5-week assimilation window length and 150 ensembles. Assimilating more observations (e.g., satellite observed CO_2 data) or applying an advanced covariance localization method or inflation method can help to obtain similar results to those obtained by the optimum configuration with relatively reasonable computational cost.

Acknowledgements. The authors appreciate two reviewers for their valuable comments. This study was supported by the Korea Meteorological Administration Research and Development Program under Grant KMIPA2015-2021. The authors thank Andrew R. Jacobson (ESRL, NOAA, USA) for providing resources to run CarbonTracker, Motoki Sasakawa (NIES, Japan) for providing Siberian observation (JR-STATION) data, Toshinobu Machida (NIES, Japan) for providing CONTRAIL data, Atsushi Takizawa (JMA, Japan) for providing Ryori (RYO), Yonagunijima (YON), and Minamitorishima (MNM) data (available at the WDCGG homepage, http://ds.data.jma.go.jp/wdcgg/), and Hitoshi Mukai (NIES, Japan) for providing Hateruma (HAT) and Cape Ochi-ishi (COI) data.

The authors also acknowledge atmospheric CO_2 measurement data providers and cooperating agencies at China Meteorological Administration, Commonwealth Scientific and Industrial Research Organization, Environment and Climate Change Canada, Instituto de Pesquisas Energeticas e Nucleares, Lawrence Berkeley National Laboratory, National Institute of Environmental Research, National Center for Atmospheric Research, and National Oceanic and Atmospheric Administration Earth System Research Laboratory.

Edited by: Masahiro Watanabe

References

Andrews, A. E., and Coauthors, 2014: CO_2, CO, and CH_4 measurements from tall towers in the NOAA Earth System Research Laboratory's Global Greenhouse Gas Reference Network: instrumentation, uncertainty analysis, and recommendations for future high-accuracy greenhouse gas monitoring efforts. *Atmos. Meas. Tech.*, **7**, 647-687, doi:10.5194/amt-7-647-2014.

Babenhauserheide, A., S. Basu, S. Houweling, W. Peters, and A. Butz, 2015: Comparing the CarbonTracker and TM5-4DVar data assimilation systems for CO_2 surface flux inversions. *Atmos. Chem. Phys.,* **15**, 9747-9763, doi:10.5194/acp-15-9747-2015.

Baker, D. F., S. C. Doney, and D. S. Schimel, 2006: Variational data assimilation for atmospheric CO_2. *Tellus,* **58**, 359-365.

Ballav, S., and Coauthors, 2012: Simulation of CO_2 concentration over East Asia using the regional transport model WRF-CO_2. *J. Meteor. Soc. Japan*, **90**, 959-976, doi:10.2151/jmsj.2012-607.

Basu, S., and Coauthors, 2013: Global CO_2 fluxes estimated from GOSAT retrievals of total column CO_2. *Atmos. Chem. Phys.,* **13**, 8695-8717, doi:10.5194/acp-13-8695-2013.

Battle, M., M. L. Bender, P. P. Tans, J. W. C. White, J. T. Ellis, T. Conway, and R. J. Francey, 2000: Global carbon sinks and their variability inferred from atmospheric O_2 and $\delta^{13}C$. *Science*, **287**, 2467-2470.

Betts, R. A., C. D. Jones, J. R. Knight, R. F. Keeling, and J. J. Kennedy, 2016: El Niño and a record CO_2 rise. *Nat. Clim. Change*, **6**, 806-810, doi:10.1038/nclimate3063.

Bhattacharya, S. K., and Coauthors, 2009: Trace gases and CO_2 isotope records from Cabo de Rama, India. *Curr. Sci.,* **97**, 1336-1344.

Biraud, S. C., M. S. Torn, J. R. Smith, C. Sweeney, W. J. Riley, and P. P. Tans, 2013: A multi-year record of airborne CO_2 observations in the US Southern Great Plains. *Atmos. Meas. Tech.*, **6**, 751, doi:10.5194/amt-6-751-2013.

Boden, T. A., G. Marland, and R. Andres, 2010: Global, regional, and national fossil-fuel CO_2 emissions, Carbon Dioxide Information Analysis Center, doi:10.3334/CDIAC/00001_V2010, 10. [Available online at http://cdiac.ornl.gov/trends/emis/overview_2007.html.]

Bruhwiler, L. M. P., A. M. Michalak, and P. P. Tans, 2011: Spatial and temporal resolution of carbon flux estimates for 1983-2002. *Biogeosci.*, **8**, 1309-1331, doi:10.5194/bg-8-1309-2011.

Chatterjee, A., and A, M. Michalak, 2013: Technical Note: Comparison of ensemble Kalman filter and variational approaches for CO_2 data assimilation. *Atmos. Chem. Phys.,* **13**, 11643-11660, doi:10.5194/acp-13-11643-2013.

_____, A. M. Michalak, J. L. Anderson, K. L. Mueller, and V. Yadav, 2012: Toward reliable ensemble Kalman filter estimates of CO_2 fluxes. *J. Geophys. Res.,* **117**, D22306, doi:10.1029/2012JD018176.

Chevallier, F., M. Fisher, P. Peylin, S. Serrar, P. Bousquet, F.-M. Bréon, A. Chédin, and P. Ciais, 2005: Inferring CO_2 sources and sinks from satellite observations: Method and application to TOVS data. *J. Geophys. Res.,* **110**, D24309, doi:10.1029/2005JD006390.

_____, S. Maksyutov, P. Bousquet, F.-M. Bréon, R. Saito, Y. Yoshida, and T. Yokota, 2009: On the accuracy of the CO_2 surface fluxes to be estimated from the GOSAT observations. *Geophys. Res. Lett.,* **36**, L19807, doi: 10.1029/2009GL040108.

_____, and Coauthors, 2010: CO_2 surface fluxes at grid point scale estimated from a global 21 year reanalysis of atmospheric measurements. *J. Geophys. Res.,* **115**, D21307, doi:10.1029/2010JD013887.

Conway, T.J., P. M. Lang, and K. A. Masarie, cited 2011: Atmospheric Carbon Dioxide Dry Air Mole Fractions from the NOAA ESRL Carbon Cycle Cooperative Global Air Sampling Network, 1968-2010.

Engelen, R. J., S. Serrar, and F. Chevallier, 2009: Four-dimensional data assimilation of atmospheric CO_2 using AIRS observations. *J. Geophys. Res.,* **114**, D03303, doi:10.1029/2008JD010739.

Enting, I. G., 2002: *Inverse Problems in Atmospheric Constituent Transport*. Cambridge University Press, 392 pp, doi:10.1017/CBO9780511-535741.

European Commission, 2009: Emission Database for Global Atmospheric Research (EDGAR), release version 4.0. [Available online at http://edgar.jrc.ec.europa.eu/.]

Evensen, G., 1994: Sequential data assimilation with a nonlinear quasi-geostrophic model using Monte Carlo methods to forecast error statistics. *J. Geophys. Res.,* **99**, 10143-10162.

Feng, L., P. I. Palmer, H. Bösch, and S. Dance, 2009: Estimating surface CO_2 fluxes from space-born CO_2 dry air mole fraction observations using an ensemble Kalman Filter. *Atmos. Chem. Phys*., **9**, 2619-2633.

_____, P. I. Palmer, Y. Yang, R. M. Yantosca, S. R. Kawa, J.-D. Paris, H. Matsueda, and T. Machida, 2011: Evaluating a 3-D transport model of atmospheric CO_2 using ground-based, aircraft, and space-borne data. *Atmos. Chem. Phys.,* **11**, 2789-2803, doi:10.5194/acp-11-2789-2011.

Fujii, Y., 1990: An Assessment of the Responsibility for the Increase in the CO_2 Concentration and Inter-generational Carbon Accounts. IIASA Working Paper, WP-90-055, 31 pp.

Gatti, L. V., J. B. Miller, M. T. S. D'amelio, A. Martinewski, L. S. Basso, M. E. Gloor, S. Wofsy, and P. Tans, 2010: Vertical profiles of CO_2 above eastern Amazonia suggest a net carbon flux to the atmosphere and balanced biosphere between 2000 and 2009. *Tellus*, **62**, 581-594, doi:10.1111/j.1600-0889.2010.00484.x.

Gurney, K. R., and Coauthors, 2002: Towards robust regional estimates of CO_2 sources and sinks using atmospheric transport models. *Nature,* **415**, 626-630.

Hamill, T. M., 2001: Interpretation of rank histograms for verifying ensemble forecasts. *Mon. Wea. Rev.,* **129**, 550-560.

Houtekamer, P. L., and H. L. Mitchell, 1998: Data assimilation using an Ensemble Kalman Filter technique. *Mon. Wea. Rev.,* **126**, 796-811.

Houweling, S., and Coauthors, 2015: An intercomparison of inverse models for estimating sources and sinks of CO_2 using GOSAT measurements. *J. Geophys. Res.*, **120**, 5253-5266, doi:10.1002/2014JD022962.

Jacobson, A. R., S. E. M. Fletcher, N. Gruber, J. L. Sarmiento, and M. Gloor, 2007: A joint atmosphere-ocean inversion for surface fluxes of carbon dioxide: 2. Regional results. *Glob. Biogeochem. Cycles,* **21**, GB1019, doi:10.1029/2006GB002703.

Ju, O.-J., J.-S. Cha, D.-W. Lee, Y.-M. Kim, J.-Y. Lee, and I.-S. Park, 2007: Analysis of variation characteristics of greenhouse gases in the background atmosphere measured at Gosan, Jeju. *J. Korean Soc. Atmos. Environ.*, **23**, 487-497 (in Korean with English abstract).

Kim, H., H. M. Kim, J. Kim, and C.-H. Cho, 2016: A comparison of the atmospheric CO_2 concentrations obtained by an inverse modeling system and passenger aircraft based measurement. *Atmosphere,* **26**, 387-400, doi:10.14191/Atmos.2016.26.3.387 (in Korean with English abstract).

Kim, J., H. M. Kim, and C.-H. Cho, 2012: Application of Carbon Tracking System based on ensemble Kalman filter on the diagnosis of Carbon Cycle in Asia. *Atmosphere*, **22**, 415-427, doi:10.14191/Atmos.2012.22.

4.415 (in Korean with English abstract).

_____, _____, and _____, 2014a: The effect of optimization and the nesting domain on carbon flux analysis in Asia using a carbon tracking system based on the ensemble Kalman filter. *Asia-Pac. J. of Atmos. Sci.,* **50**, 327-344, doi:10.1007/s13143-014-0020-y.

_____, _____, and _____, 2014b: Influence of CO_2 observations on the optimized CO_2 flux in an ensemble Kalman filter. *Atmos. Chem. Phys.,* **14**, 13515-13530, doi:10.5194/acp-14-13515-2014.

_____, _____, _____, K.-O. Boo, A. R. Jacobson, M. Sasakawa, T. Machida, M. Arshinov, and N. Fedoseev, 2017: Impact of Siberian observations on the optimization of surface CO_2 flux, *Atmos. Chem. Phys.,* **17**, 2881-2899, doi:10.5194/acp-17-2881-2017.

Krinner, G., N. Viovy, N. de Noblet-Ducoudré, J. Ogée, J. Polcher, P. Friedlingstein, P. Ciais, S. Sitch, and I. Colin Prentice, 2005: A dynamic global vegetation model for studies of the coupled atmosphere-biosphere system. *Global Biogeochem. Cycles*, **19**, GB1015, doi:10.1029/2003 GB002199.

Krol, M., S. Houweling, B. Bregman, M. van den Broek, A. Segers, P. van Velthoven, W. Peters, F. Dentener, and P. Bergamaschi, 2005: The two-way nested global chemistry-transport zoom model TM5: Algorithm and applications. *Atmos. Chem. Phys.,* **5**, 417-432.

Law, R. M., and Coauthors, 2008: TransCom model simulations of hourly atmospheric CO_2: Experimental overview and diurnal cycle results for 2002. *Global Biogeochem. Cycles*, **22**, GB3009, doi:10.1029/2007GB-003050.

Langenfelds, R. L., R. J. Francey, B. C. Pak, L. P. Steele, J. Lloyd, C. M. Trudinger, and C. E. Allison, 2002: Interannual growth rate variations of atmospheric CO_2 and its $\delta^{13}C$, H_2, CH_4 and CO between 1992 and 1999 linked to biomass burning. *Global Biogeochem. Cycles*, **16**, doi:10.1029/2001GB001466.

Liu, L., L. Zhou, X. C. Zhang, M. Wen, F. Zhang, B. Yao, and S. X. Fang, 2009: The characteristics of atmospheric CO_2 concentration variation of four national background stations in China. *Sci. China, Ser. D*, **52**, 1857-1863.

Liu, Z., and Coauthors, 2015: Reduced carbon emission estimates from fossil fuel combustion and cement production in China. *Nature*, **524**, 335-338, doi:10.1038/nature1467.

Machida, T., and Coauthors, 2008: Worldwide measurements of atmospheric CO_2 and other trace gas species using commercial airlines. *J. Atmos. Oceanic Technol.*, **25**, 1744-1754, doi:10.1175/2008JTECHA-1082.1.

Masarie, K. A., W. Peters, A. R. Jacobson, and P. P. Tans, 2014: ObsPack: A framework for the preparation, delivery, and attribution of atmospheric greenhouse gas measurements. *Earth Syst. Sci. Data*, **6**, 375-384, doi:10.5194/essd-6-375-2014.

Meirink, J. F., P. Bergamaschi, and M. C. Krol, 2008: Four-dimensional variational data assimilation for inverse modelling of atmospheric methane emissions: Method and comparison with synthesis inversion. *Atmos. Chem. Phys.,* **8**, 6341-6353, doi:10.5194/acp-8-6341-2008.

Mukai, H., and Coauthors, 2001: Characterization of atmospheric CO_2 observed at two-background air monitoring stations (Hateruma and Ochi-ishi) in Japan. *Proc. Sixth International Carbon Dioxide Conference, Sendai*, Japan, 1-5.

_____, and Coauthors, 2014a: Continuous observational data of atmospheric CO_2 mixing ratios on Cape Ochi-ishi, Ver. 1.0. National Institute for Environmental Studies, doi:10.17595/20160901.002.

_____, and Coauthors, 2014b: Continuous observational data of atmospheric CO_2 mixing ratios on Hateruma island, Ver. 1.0. National Institute for Environmental Studies, doi:10.17595/20160901.001.

Niwa, Y., T. Machida, Y. Sawa, H. Matsueda, T. J. Schuck, C. A. M. Brenninkmeijer, R. Imasu, and M. Satoh, 2012: Imposing strong constraints on tropical terrestrial CO_2 fluxes using passenger aircraft based measurements. *J. Geophys. Res.,* **117**, D11303. doi:10.1029/2012JD017474.

Olson, J. S., J. A. Watts, and L. J. Allison, 1985: Major World Ecosystem Complexes Ranked by Carbon in Live Vegetation: A Database. NDP017, Carbon Dioxide Information Analysis Center, doi:10.3334/CDIAC/lue.ndp017.

Pan, Y., and Coauthors, 2011: A large and persistent carbon sink in the world's forests. *Science*, **333**, 988-993, doi:10.1126/science.1201609.

Park, J. I., and H. M. Kim, 2010: Typhoon Wukong (200610) prediction based on the ensemble Kalman filter and ensemble sensitivity analysis. *Atmosphere,* **20**, 287-306 (in Korean with English abstract).

Patil, D. J., B. R. Hunt, E. Kalnay, J. A. Yorke, and E. Ott, 2001: Local low dimensionality of atmospheric dynamics. *Phys. Rev. Lett.*, **86**, 5878-5881.

Patra, P., and Coauthors, 2008: TransCom model simulations of hourly atmospheric CO_2: Analysis of synoptic-scale variations for the period 2002-2003. *Global Biogeochem. Cycles*, **22**, GB4013, doi:10.1029/2007GB003081.

Peters, W., J. B. Miller, J. Whitaker, A. S. Denning, A. Hirsch, M. C. Krol, D. Zupanski, L. Bruhwiler, and P. P. Tans, 2005: An ensemble data assimilation system to estimate CO_2 surface fluxes from atmospheric trace gas observations. *J. Geophys. Res.,* **110**, D24304, doi:10.1029/2005JD006157.

_____, and Coauthors, 2007: An atmospheric perspective on North American carbon dioxide exchange: CarbonTracker. *Proc. Nat. Acad. Sci. USA.,* **104**, 18925-18930, doi:10.1073/pnas.0708986104.

_____, and Coauthors, 2010: Seven years of recent European net terrestrial carbon dioxide exchange constrained by atmospheric observations. *Glob. Change Biol*., **16**, 1317-1337, doi:10.1111/j.1365-2486.2009.02078.x.

Peylin, P., and Coauthors, 2013: Global atmospheric carbon budget: results from an ensemble of atmospheric CO_2 inversions. *Biogeosci.*, **10**, 6699-6720, doi:10.5194/bg-10-6699-2013.

Rayner, P. J., M. Scholze, W. Knorr, T. Kaminski, R. Giering, and H. Widmann, 2005: Two decades of terrestrial carbon fluxes from a carbon cycle data assimilation system (CCDAS). *Global Biogeochem. Cycles*, **19**, GB2026, doi:10.1029/2004GB002254.

Sasakawa, M., and Coauthors, 2010: Continuous measurements of methane from a tower network over Siberia. *Tellus,* **62**, 403-416, doi:10.1111/j.1600-0889.2010.00494.x.

_____, T. Machida, N. Tsuda, M. Arshinov, D. Davydov, A. Fofonov, and O. Krasnov, 2013: Aircraft and tower measurements of CO_2 concentration in the planetary boundary layer and the lower free troposphere over southern taiga in West Siberia: Long-term records from 2002 to 2011. *J. Geophys. Res.*, **118**, 9489-9498, doi:10.1002/jgrd.50755.

Sheu, G.-R., N.-H. Lin, J.-L. Wang, and C.-T. Lee, 2009: Lulin atmospheric background station: A new high-elevation baseline station in Taiwan. *EarozoruKenyu*, **24**, 84-89, doi:10.11203/jar.24.84 (in Japanese).

Stephens, B. B., N. L. Miles, S. J. Richardson, A. S. Watt, and K. J. Davis, 2011: Atmospheric CO_2 monitoring with single-cell NDIR-based analyzers. *Atmos. Meas. Tech.*, **4**, 2737, doi:10.5194/amt-4-2737-2011.

Thompson, R. L., and Coauthors, 2016: Top-down assessment of the Asian carbon budget since the mid 1990s. *Nat. Commun*., **7**, 10724, doi:10.1038/ncomms10724.

Tsutsumi, Y., K. Mori, M. Ikegami, T. Tashiro, and K. Tsuboi, 2006: Long-term trends of greenhouse gases in regional and background events observed during 1998-2004 at Yonagunijima located to the east of the Asian continent. *Atmos. Environ.*, **40**, 5868-5879.

van der Werf, G. R., and Coauthors, 2010: Global fire emissions and the contribution of deforestation, savanna, forest, agricultural, and peat fires (1997-2009). *Atmos. Chem. Phys.,* **10**, 11707-11735, doi:10.5194/acp-10-11707-2010.

Whitaker, J. S., and T. M. Hamill, 2002: Ensemble data assimilation

without perturbed observations. *Mon. Wea. Rev.,* **130**, 1913-1924.

World Meteorological Organization (WMO), 2016: Greenhouse gas bulletin: The state of greenhouse gases in the atmosphere based on global observations through 2015. [Available online at https://library.wmo.int/opac/doc_num.php?explnum_id=3084.]

Worthy, D. E. J., A. Platt, R. Kessler, M. Ernst, and S. Racki, 2003: The greenhouse gases measurement program, measurement procedures and data quality. Canadian Baseline Program, Quebec, 97-120.

Zhang, H. F., and Coauthors, 2014a: Net terrestrial CO_2 exchange over China during 2001-2010 estimated with an ensemble data assimilation system for atmospheric CO_2. *J. Geophys. Res.,* **119**, 3500-3515, doi:10.1002/2013JD021297.

_____, and Coauthors, 2014b: Estimating Asian terrestrial carbon fluxes from CONTRAIL aircraft and surface CO_2 observations for the period 2006-2010. *Atmos. Chem. Phys*., **14**, 5807-5824, doi:10.5194/acp-14-5807-2014.